ELSEVIER

Contents lists available at ScienceDirect

International Journal of Solids and Structures

journal homepage: www.elsevier.com/locate/ijsolstr





A transient simulation of thermomechanical instability in metal-free friction materials with anisotropic properties

Kingsford Koranteng*, Joseph-Shaahu Shaahu, Yun-Bo Yi

Department of Mechanical and Materials Engineering, University of Denver, Denver, CO 80208, USA

ARTICLE INFO

Keywords:
Metal-free
Friction material
Thermomechanical instability
Growth rate
Pressure perturbation

ABSTRACT

A two-dimensional non-linear transient thermomechanical model is developed to incorporate the anisotropic properties of a metal-free friction material sliding against a steel disc using a finite element approach. The main focus of the study is the effect of material anisotropy on thermomechanical instability (TMI) of friction linings used in automotive disc clutches or brakes. The model is validated by comparing the result to an existing eigenvalue solution. A parametric study on the material anisotropy revealed that for contact with the separation effect, an increase in elastic modulus E_{11} in the sliding direction and thermal conductivity K_{22} in the thickness direction discourage TMI formation. Conversely, a higher thermal conductivity K_{11} in the sliding direction and elastic modulus E_{22} in the thickness direction make the friction material more susceptible to TMI formation for a full-contact regime and contact with the separation effect. In addition, the effect of the thermal expansion coefficient was considered in this work.

1. Introduction

Thermomechanical instability (TMI) involves the coupling between different physical fields which covers the traditional thermoelastic instability, and several distinct physical interactions such as wear, convective cooling, material nonlinearities including viscoelasticity, etc. The subject has become important to manufacturers because the response of sliding systems involves several of these distinct physical fields. In sliding interactions, frictional material properties have been found to influence TMI significantly. Depending on the material properties involved in the contact interactions, the resulting temperature distributions may be highly non-uniform leading to thermoelastic distortion (Barber, 1969). This in turn influences the contact pressure distribution and eventually causes the system to be unstable (Lee and Dinwiddie, 1998). For centuries, the automobile industry has employed the use of metals such as copper to enhance the thermal properties of friction materials to minimize the onset of TMI in friction pairs during sliding interaction. While the added metals may provide a thermal benefit, it tends to harm our environment directly and indirectly. For example, copper particles produced because of wear end up polluting the soil and water bodies. Eventually harming aquatic organisms when they find their way into our water bodies by agents of erosion (Chiou and Hsu, 2019; Malhotra et al., 2020). The present situation has prompted

researchers to switch to the use of metal-free friction materials.

Prior to the existence of metal-free friction materials, several works on TEI (thermoelastic instability) and TMI models; their associated factors such as material properties, surface roughness, wear, etc. have been studied in relation to homogenous metallic materials. For example, models have been developed to estimate the onset of TEI in a friction pair on the condition that if the sliding speed of the system exceeds a certain critical value, then instability occurs. This approach was pioneered by Burton et al. (1973). It involves imposing a harmonic perturbation in the form of pressure or temperature between the sliding surface and observing the growth of the perturbation. Instability of the system occurs when the imposed perturbation grows without bound. The effects of these are hotspot formations, wear, noise, vibration, and material damage on the disc (Anderson and Knapp, 1990; Kao et al., 2000). Moreover, Anderson and Knapp (1990); Azarkhin and Barber (1986); Jang and Khonsari (2003) have shown that, when a small harmonic perturbation is imposed between two half-planes, the planes become unstable when the sliding speed exceeds a certain critical speed. Lee and Barber (1993) extended this approach to the case of a layer with a finite thickness sliding between two half-planes. In addition, an analytical model for the symmetric and antisymmetric modes was developed by Jang and Khonsari (2003) to analyze the contact between an insulator and a conductor. It was revealed that critical speed is

E-mail address: Kingsford.koranteng@du.edu (K. Koranteng).

^{*} Corresponding author.

governed by five independent dimensionless parameters. The authors also employed the condition that thermoelastic instability occurs when the sliding speed exceeds a critical value to determine the threshold of thermoelastic instability in friction pairs by including the surface roughness effect (Jang and Khonsari, 1999).

Most works on instability in sliding materials are based on the eigenvalue approach. Meanwhile, the non-linear transient modal approach is recommended because it provides an efficient numerical algorithm for the analysis of TMI (Li and Barber, 2008). Unlike the eigenvalue approach which requires that contact must be conforming, the transient approach deals with nonlinearities such as surface separation, wear effect, asperity contact, etc. in the process. A simple approach to the transient solution of TEI was carried out by Al-Shabibi and Barber (2002) using a truncated series approach (reduced-order models). Also, the fast speed expansion method could be used as carried out by Li and Barber (2008). Meanwhile, to ensure accuracy, a straightforward approach is to use a finite element discretization method. This method is preferable since it can be implemented in finite element analysis (FEA) software such as ABAQUS and ANSYS. An early attempt at using the numerical approach to study TEI was made by Kennedy and Ling, (1974). In addition, Zagrodzki, (1990) used the numerical FEA approach to investigate the transient thermomechanical phenomena for multi-disk clutch. Further, the non-linear behavior of a sliding system with TEI has been studied by Zagrodzki et al. (2001). The authors investigated the migration speed generated during sliding contact.

In this work, a non-linear transient solution to TMI is developed to investigate the response of a metal-free friction material whose properties are not invariant with respect to direction. The ultimate objective of this study, and a major distinction between this and prior work, is to investigate the effect of material anisotropy of metal-free friction materials on TMI by considering a carbon-fiber-reinforced hybrid composite friction material and using a non-linear transient approach to investigate TMI during sliding interactions. Existing research works on material influence on TMI are usually based on materials with homogenous properties. Moreover, the increasing demand for metal-free friction materials to replace copper friction materials requires a proper understanding of the material response to TMI. An attempt to study the influence of material properties on TMI was carried out by Zhao et al. (2015). In the study, the authors studied the effects of thermal conductivities, elastic moduli, and expansion coefficient on TEI based on the eigenvalue approach. More importantly, the effects of these properties in the various directions (longitudinal and transverse directions) as in the case of anisotropic material were not considered. The present study considers the influence of properties of metal-free friction material in both longitudinal and transverse directions on TMI using a transient approach with the incorporation of surface separation effects as observed in practice, and with a full-contact regime.

2. Metal-free friction material

A Carbon fiber-reinforced hybrid composite friction material made of woven fiber yarn is used in this study. The material is considered metal-free since it has no metal compositions. The mechanical stiffness matrix and thermal properties of this material are obtained using the rule of mixture by modifying the friction material presented by Biczó et al. (2020), to exclude the copper component. Moreover, because the TMI model of interest is a two-dimensional configuration, material parameters in the x-direction (longitudinal) and y-direction (transverse) were considered. The longitudinal direction is the sliding direction while the transverse direction is the thickness direction that is normal to the sliding surface. Table 1 shows the mechanical and thermal properties of the metal-free friction material used in the TMI analysis.

It is important to note that the range of the parametric study in this work is based on the carbon-fiber-reinforced hybrid composite friction material (metal-free) used. The elastic modulus values lie between 9 and

Table 1

Mechanical and thermal properties of the carbon-fiber-reinforced composite friction material

Thermomechanical properties of the metal-free friction material	
Elastic modulus (GPa)	
Longitudinal E_{11}	9,10,11,12
Transversal E_{22}	9,10,11,12
Shear modulus, G ₁₂ (GPa)	7.6
Poisson's ratio,v ₁₂	0.4
Thermal conductivity (W/(m·K))	
Longitudinal K_{11}	1,2,3,4
Transversal K_{22}	1,2,3,4
Coeff. of thermal expansion (10 ⁻⁶ C ⁻¹)	
Longitudinal α_{11}	10,11,12,13
Transversal α_{22}	10,11,12,,13

11GPa; thermal conductivity is between 1 and 4 W/m·K and the coefficient of thermal expansion is from 10 to 13 μ C⁻¹.

3. TMI model formulation

A friction disc block of material properties listed in Table 1 and a steel disc block whose properties are presented in Table 2 were used for the TMI analysis. Both blocks are considered elastic and thermally conducting. Fig. 1 shows the schematic of the two-disc blocks of different materials. Block 1 is the composite friction material while Block 2 is the conducting steel disc. Block 1 moves in-plane with a sliding speed V with respect to Block 2. Moreover, Block 1 can move in both the x and y directions while Block 2 is constrained to move in the y-direction. The two blocks have equal lengths L and heights of h_1 and h_2 respectively. When $y=y_1$, it represents the contact interface between the two blocks.

3.1. Heat transfer formulation (thermal analysis)

The general form of the two-dimensional transient conduction equation for both discs in the Cartesian coordinate system is described as:

$$\frac{\partial}{\partial x} \left(K_i \frac{\partial T_i}{\partial x} \right) + \frac{\partial}{\partial y} \left(K_i \frac{\partial T_i}{\partial y} \right) = \rho_i C_i \left(\frac{\partial T_i}{\partial t} + V_i \frac{\partial T_i}{\partial x} \right) \tag{1}$$

where C, ρ , V, K denote the specific heat, density, sliding speed, and conductivity, respectively. Also, the subscript i=1, 2. When i=1, it denotes the expression for the friction plate where $V_1=V$. Further, when i=2, it denotes the conduction equation for the disc where $V_2=0$.

During sliding contact between the two blocks, the heat generated at the contact surface is defined by:

$$q = fVP_i, \quad i = 1, 2 \tag{2}$$

where f is the friction coefficient; V = Sliding velocity (m/s) and P is the contact pressure (Pa) at the interface.

3.1.1. Convective term/convergence problem

The dual conductive-convective nature of Eq. (1) can cause a serious convergence problem with numerical solutions when the standard

Table 2Material properties of the conducting material used in this analysis.

Properties	Conducting material (Steel)
Modulus of Elasticity, E (GPa)	210
Conductivity, K (W/(m·K))	57
Poisson's ratio, v	0.4
Coeff. of thermal expansion (10 ⁻⁶ C ⁻¹)	12
Density, $\rho(\mathbf{kg}/m^3)$	7250
Specific heat, C(J·kg ⁻¹ ·K ⁻¹)	460

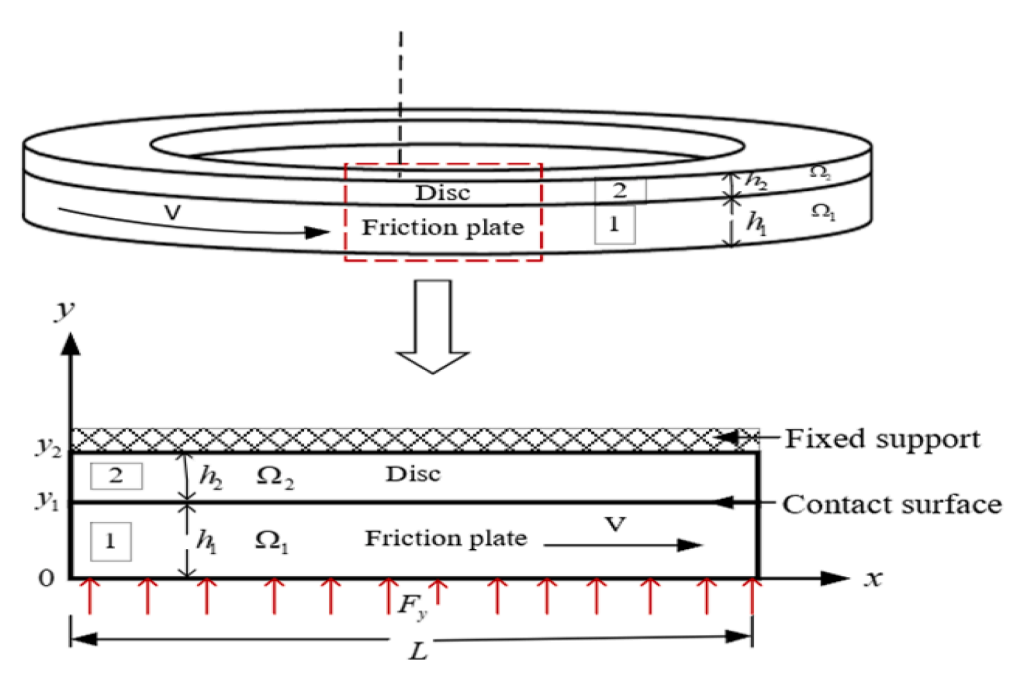


Fig. 1. Schematic of the sliding components.

Galerkin finite element approach is used. This is because it does not accurately discretize the convective term $V\frac{\partial T}{\partial x}$. For instance, if the Peclet number is greater than 2, the algorithm shows numerical oscillations in the solution that become physically meaningless. Meanwhile, for clutch and brake models, the Peclet number is usually greater than 100. To address this convective problem, we employed the Petrov-Galerkin algorithm that uses an upwinding approach (Heinrich et al., 1977; Yu and Heinrich, 1987), where the central-difference scheme is replaced with the backward-difference scheme for the dual conductive-convective term. It works by using the non-symmetric weighing functions in the finite element by maintaining the same shape functions as in the case of the standard Galerkin finite element method. In this analysis, the commercial finite element package ABAQUS was utilized (Smith, 2009) which is equipped with the aforementioned Petrov-Galerkin algorithm.

3.1.2. Boundary conditions

If the surfaces $y = y_1$ are in perfect contact, the clearance $\Delta u_{y_1} = 0$ and the surface boundary condition is given implicitly by the energy conservation condition as:.

$$K_1 \frac{\partial T_1}{\partial y} \Big|_{y=y_1} - K_2 \frac{\partial T_2}{\partial y} \Big|_{y=y_1} = q \tag{3}$$

When separation occurs in certain regions at the sliding interface, the heat generation is zero at that region since $P_i = 0$. Therefore, it was assumed that there would be no heat conduction across the gap when separation occurs. This is given by:

$$\left. \frac{\partial T_1}{\partial y} \right|_{y=y_1} = \left. \frac{\partial T_2}{\partial y} \right|_{y=y_1} = 0 \tag{4}$$

Also, surface film conditions Ω_i (0.5 W/m^2K), where i=1,2, were introduced at an ambient temperature of 273 K on the two exposed edges of the model due to the heat exchange with the environment as shown in Fig. 1, giving:

$$-K_{1}\frac{\partial T_{1}}{\partial y}\bigg|_{y=0} = \Omega_{1}(T(x,0) - T_{o}); K_{2}\frac{\partial T_{2}}{\partial y}\bigg|_{y=0} = \Omega_{2}(T(x,y_{2}) - T_{o})$$
 (5)

This is very important to prevent heat build-up due to the absence of heat loss. Further, at x=0 and x=L, cyclic, symmetrical boundary conditions were imposed on the two sides of the disc blocks. This was

done to ensure that the temperatures at the two opposite edges of each block are the same to depict the sliding behavior of two complete circular discs instead of two sliding blocks.

$$T_1|_{x=0}(y,t) = T_1|_{x=L}(y,t) \text{ and } T_2|_{x=0}(y,t) = T_2|_{x=L}(y,t)$$
 (6)

3.2. Mechanical formulation (static elastic analysis)

The general elastic contact in ABAQUS was used to compute the resulting pressures during the contact of the two sliding blocks. With reference to Fig. 1, at the edges y = 0 and $y = y_2$, the following boundary conditions were imposed.

$$(u_y)_1 \big|_{y=0} = 0 \text{ and } (u_y)_2 \big|_{y=0} = \text{Constant}$$
 (7)

where u_{y} denotes the displacement of the nodes in the y-direction.

Also, an external force F_y was applied at the boundary condition to serve as a control in the y-direction by keeping the two blocks in contact without a sudden separation. Moreover, at the side edges of the blocks where x = 0 and x = L, cyclic symmetry boundary conditions were defined for the displacement of the nodes in the x and y-directions. This was to depict the behavior of the sliding of two complete circular discs.

$$(u_x)_{1,2}\Big|_{x=0} = (u_x)_{1,2}\Big|_{x=L} \text{ and } (u_y)_{1,2}\Big|_{x=0} = (u_y)_{1,2}\Big|_{x=L}$$
 (8)

Further, at $y = y_2$, Block 2 was constrained to prevent it from moving further away in the positive y-direction due to the externally applied force F_y .

3.3. Finite element mesh

Considering the two sliding bodies, the perturbation in contact pressure or temperature moves at a relatively high velocity close to the sliding velocity V, with respect to the poor conductor. Therefore, it was assumed there is a high possibility that the Peclect number associated with the friction material would be high and may lead to a high-temperature gradient in the y-direction near the contact surface (Al-Shabibi and Barber, 2002; Zagrodzki et al., 2001), hence the need to perform mesh refinement, especially near the interface. The finite element mesh of the poor conductor was biased at 1.25 close to the contact surface and a mesh refinement was carried out to ensure that the

model was capable of reproducing a strong variation of temperature in the skin layer by estimating the temperature distribution perpendicular to the interface (Zagrodzki et al., 2001). From Fig. 2, It can be observed that the temperature perturbation in the y-direction normal to the contact surface is fully captured by the mesh points of the poor conductor by using a total of 750 elements.

In the thermal analysis, a 4-node convection/diffusion quadrilateral (DCC2D4)) element type was used for the friction material. This was done to introduce a convective term to the moving block 1 while a 4-node linear heat transfer quadrilateral (DC2D4) element type was used for the non-moving conductor material (block 2). Meanwhile, In the elastic part of the analysis, a 4-node bilinear plane strain quadrilateral (CPE4) element type was used for both the conducting and non-conducting materials.

4. Solution to the TMI model formulation

• Start by defining a small sinusoidal perturbation of a specific wavenumber ($m=2n\pi/L$), on the mean contact pressure, P_m . Here, n is the number of hotspots. The perturbation could be any noise imposed on the mean contact pressure. This noise can always be decomposed into Fourier series where each term is a sinusoidal wave. Therefore, the sinusoidal wave can directly be added to the mean pressure as a form of noise and imposed on the contact interface between the two sliding bodies.

$$p(x,t) = P_m + A\sin(\omega x + \phi) \tag{9}$$

where P_m is the mean pressure and the remaining term represents the harmonic pressure perturbation; A is the amplitude of the perturbation; x is the distance (m); \emptyset is the phase angle; ω is the angular velocity (rad/s).

Equation (2) is then used to compute the frictional heat generated by using the variable contact pressure obtained from Eq. (9). Similarly, the mass flow is computed using the density, ρ of the composite friction material, and the sliding velocity, V.

- A transient heat analysis is carried out using ABAQUS code and the resulting nodal temperatures are extracted from the contacting interface at $y = y_1$. The extracted nodal temperatures are fed into the elastic part of the analysis.
- In the thermomechanical analysis, the resulting pressure distribution is extracted from the contact interface and the new nodal contact

pressure is used to compute the heat flux for the next transient heat analysis.

- The process is repeated using an iterative scheme established using MATLAB. In the process, both the amplitude of the perturbation and the location of its peak pressure in the sliding direction will change until the solution converges where the form of the perturbation and its location remains unchanged within a specified accuracy through a single iteration.
- If the sliding speed is below the critical speed, the expected contact pressures decay at each iteration and converge to uniform contact pressure. Meanwhile, when the sliding speed V is above the critical speed V_c , the imposed pressure perturbation grows and eventually reaches a condition where some nodes separate. However, in this work, it was ensured that the sliding speed V was greater than the critical speed V_c at the start of the analysis, so that it could be determined how the material properties affect TMI. Fig. 3 illustrates the entire iterative process.

4.1. Validation of the model

The condition under which the imposed sinusoidal perturbation on the constant pressure grows exponentially with time was examined. If this condition is satisfied, it can be concluded that thermomechanical instability has occurred since the perturbation grows exponentially without bound. Here, the expression for the contact pressure with time can be written as:

$$p(x,t) = P_m + A\sin(\omega x + \phi)e^{bt}$$
(10)

where *b* is the growth rate.

The mean pressure remains constant while the imposed perturbation grows. For a stable system, the growth rate is expected to decay with time. Dividing both sides of Eq. (10) by the mean pressure gives:

$$\frac{p(x,t)}{P_m} = 1 + \frac{A}{P_m} \sin(\omega x + \phi) e^{bt}$$
(11)

From Eq. (11), it was assumed that the first term on the right is significantly small compared to the second term if TMI occurs. Therefore, the first term on the right was excluded. Taking the natural logarithm of both sides of the remaining expression, an equation of a straight line is obtained, where the slope of the line represents the growth rate, b. The condition for instability occurs when the slope of the line is positive.

Fig. 4(a) shows the exponential growth of pressure perturbation at

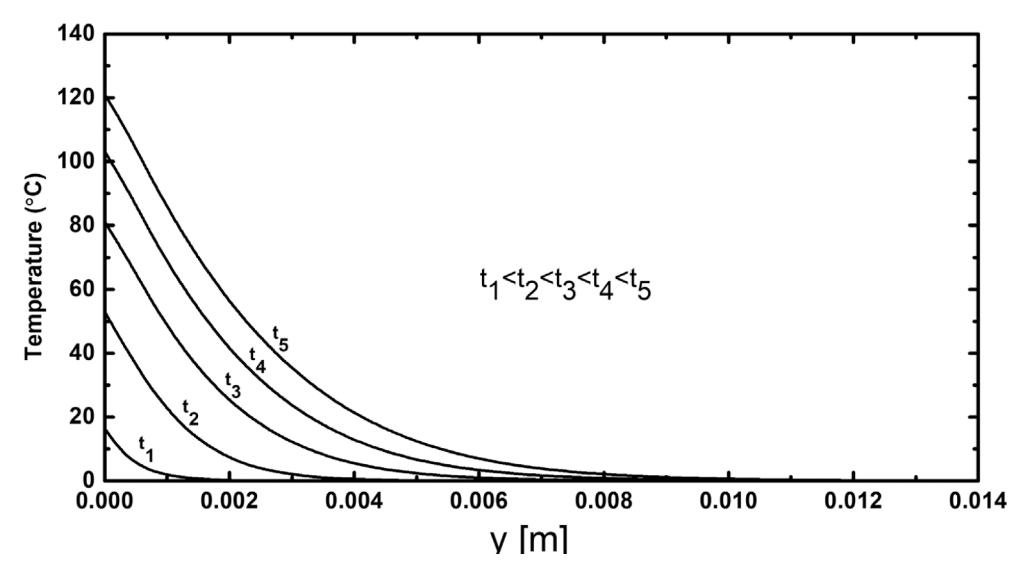


Fig. 2. Character of temperature distribution in the skin layer of the finite mesh of the poor conductor.

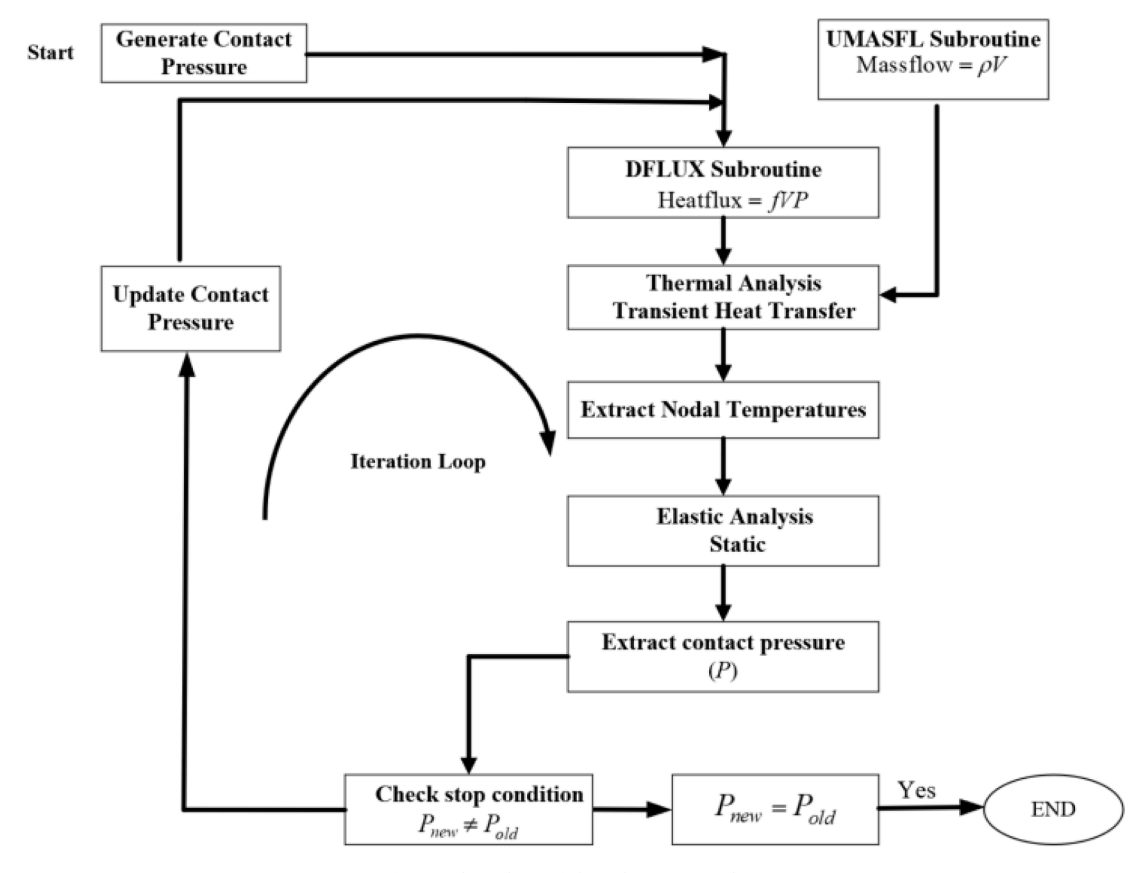
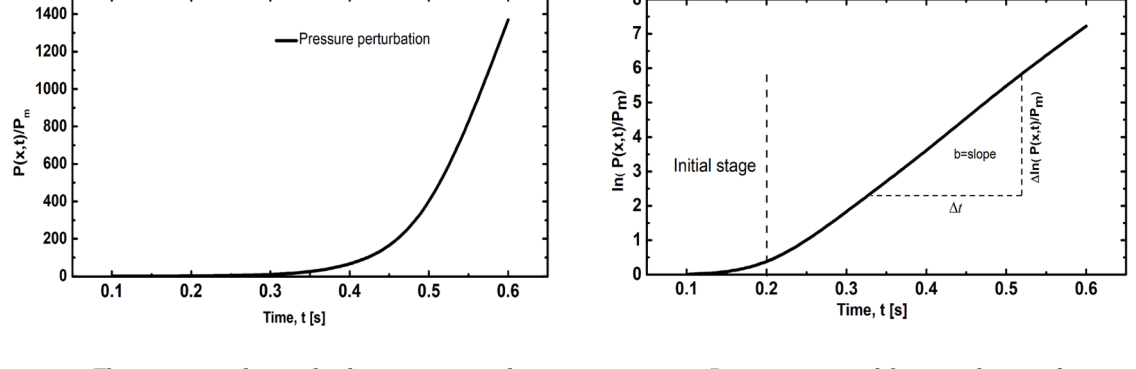


Fig. 3. Flow chart of the solution procedure.



a) The exponential growth of pressure perturbation with time, t [s]

b) Determination of the growth rate of pressure perturbation

Fig. 4. (a) Exponential growth of contact pressure; and (b) Natural logarithm of the contact pressure perturbation as a function of time.

different instants for a speed of 3.0 m/s. It is observed that the perturbation grows exponentially, thus the system is unstable, and therefore, thermomechanical instability has been initiated. A plot of the natural logarithm of the variable pressure divided by the mean pressure is a straight line with a positive slope as seen in Fig. 4(b). The slope represents the growth rate of the pressure perturbation. Also, it was noted that a particular mode of the perturbation is triggered at the initial stages that reflected only the general pattern of the eigenmode. The actual mode forms gradually during the initial step.

4.1.1. Comparison with eigenvalue approach

The model was validated by comparing the result of the developed algorithm involving a full-contact regime with the results of an eigenvalue approach using Hotspotter (Yi and Barber, 2001). It is open-source

software designed to closely approximate the growth rate, critical speed, and the number of hotspot formations in sliding systems. The material properties listed in Table 1 were used. Moreover, Hotspotter only permits the entry of isotropic material property for the thermal conductivity, hence the effective thermal conductivity was computed and applied in Hotspotter. A friction coefficient of 0.2 was assumed in both models. Fig. 5 presents the comparison of the growth rate against velocity for the two models. The results from the developed transient model agree extremely well with the results from Hotspotter for a full-contact regime analysis. The accuracy of the present model provides confidence in the output results from the simulations carried out in this work.

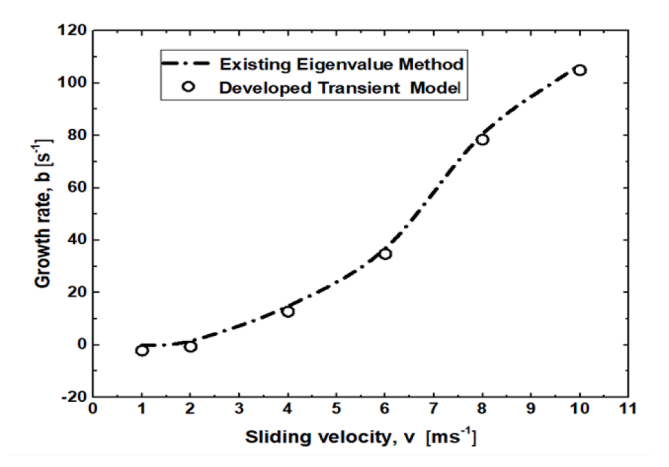


Fig. 5. Comparison of growth rate vs. sliding velocity for the existing eigenvalue method and the currently developed model.

4.2. TMI without separation (Full-contact regime)

Here, a full-contact engagement without any separation was considered. Thus, the model assumes that all contact surface nodes remain in complete contact throughout the sliding process. Therefore, since full contact is retained without separation, the thermomechanical problem becomes linear. This is similar to the eigenvalue approach used in the early study of thermoelastic instability (Burton et al., 1973; Dow and Burton, 1972), which was further improved by Yi et al. (2000) using a finite element implementation method. In this work, the full contact regime analysis was performed using ABAQUS code to investigate the dominant material parameter in TMI formation. The sliding speed was kept constant at V = 3.0 m/s and the simulation was carried out for a total time of t = 80 s with a step time $\Delta t \le 4.10^{-4}$ s, computed using a Courant number $Cu = V\Delta t/h_x \le 1$, where h_x is the mesh size in the xdirection. The simulation was carried out using a specified time in this case because the problem is linear and there is no node separation due to non-linearity. Therefore pressure and temperature may continue to grow exponentially leading to very high peak values, thus the need to terminate the iteration process after a specific time period.

4.3. TMI with contact separation

In practice, the thermomechanical behavior of clutch and brakes is non-linear due to the loading, geometry, and material non-linearity. Therefore, it is important to consider the separation effect because above certain temperatures, the problem may involve regions of separation. For separation to occur, the imposed harmonic perturbation increases at each iteration, creating a condition where some contact nodes start to separate. This is usually accompanied by a rapid contraction of the contact area and a corresponding increase in the maximum contact pressure due to flash temperatures. The phenomenon may be due to the local reduction or constriction to the path where heat is generated which increases the density of thermal flux lines at the contact spot, causing thermal spikes that represent the hotspot formation on the discs. The amplitude of the perturbation will continue to increase at the contact surface as more nodes separate with further iterations until the solution converges where the form of the perturbation and its location remains unchanged using a step time $\Delta t \leq 4.10^{-4}$ s. The non-uniform contact pressure distribution on the contact surface leads to the non-uniform distribution of temperature that causes hotspots, judder, and thermal buckling as observed on brake and clutch discs (Koranteng et al., 2020). As mentioned earlier, material properties play a major role in TMI formation. Therefore, a non-linear steady-state solution is considered by allowing surface separation and investigating the effects of the dominant material properties.

5. Results/discussions

5.1. Effect of thermal conductivity

Thermal conductivity forms an important factor relating to system stability as reported by Zhao et al. (2015). The critical speed of friction materials has been found to increase as thermal conductivity increases. This shows how important the parameters are in ensuring system stability. This work further investigates how the thermal conductivity of the friction material in the longitudinal direction and transverse direction affect the stability of the sliding system using a transient approach.

5.1.1. Longitudinal direction (K_{11})

Thermal conductivity was varied in the longitudinal direction at $K_{11}=1,2,3,4$ W/(m·K) while keeping $K_{22},E_{11},E_{22},\alpha_{11},\alpha_{22}$ at 4 W/(m·K), 11GPa, 11GPa, 13 μ C⁻¹, 13 μ C⁻¹ respectively. Fig. 6a & b show the contact pressure distribution without separation and with separation effect, respectively. Increasing the thermal conductivity K_{11} exhibited insignificant effect on the system instability. The maximum contact pressure was found to increase slightly as K_{11} increases. For a better understanding of the influence of K_{11} on TMI, the corresponding growth rates by increasing K_{11} were computed. The growth rate, b (s⁻¹) of contact pressure at $K_{11}=1,2,3,4$ W/(m·K) were found to be 0.126, 0.269, 0.2670 and 0.2671, respectively. This shows that, increasing K_{11} causes the growth rate to increase slightly, leading to a reduction in the critical speed which makes the system unstable.

5.1.2. Transverse direction/Thickness direction (K_{22})

The thermal conductivity in the transverse direction was also varied $(K_{22} = 1, 2, 3, 4W/(m \cdot K))$ while keeping all other material properties constant. Thus, keeping K_{11} , E_{11} , E_{22} , α_{11} , α_{22} at 4 W/(m·K), 11GPa, 11GPa, $13\mu\text{C}^{-1}$, $13\mu\text{C}^{-1}$ respectively. Fig. 7a & b show the resulting contact pressure distribution for contact with and without separation, respectively. The effect of contact pressure on the system stability was significant. Increasing K_{22} causes the imposed pressure perturbation to decay steadily, thereby stabilizing the system. This is more evident in the fullcontact regime Fig. 7(a). Further, if contact with separation is considered, for example Fig. 7(b), when $K_{22} = 1.0 \text{W}/(\text{m} \cdot \text{K})$ separation occurred at certain regions accompanied by a rapid contraction of the contact area at 0.52 < x/L < 0.68. The maximum value $(P(x,t)/P_m)$ exhibited is 10.96. Further increasing the $K_{22}=2,3,4\mathrm{W/(m\cdot K)}$ caused certain regions to have more contact interaction leading to the evolution of new local maximum pressures. This is because the uniformity of the contact pressure is enhanced leading to a gradual improvement in the temperature distribution on the contact surface as seen in Fig. 8. For instance, when $K_{22}=1.0\mathrm{W/(m\cdot K)}$, the temperature is seen to be highly non-uniform. At 0 < x/L < 0.47, the temperature was approximately $T = 8^{\circ}C$, and suddenly increased rapidly to a maximum value of T =202.5°C. Meanwhile, when the thermal conductivity is increased gradually to K_{22} = 4.0W/(m· K), the temperature assumes a more uniform profile. It starts at $T=88.4^{\circ}$ C and decreases slowly to $T=13^{\circ}$ C, at $x/L=10^{\circ}$ C, at $x/L=10^{\circ}$ C and decreases slowly to $T=10^{\circ}$ C, at $x/L=10^{\circ}$ C and decreases slowly to $T=10^{\circ}$ C, at $x/L=10^{\circ}$ C and decreases slowly to $T=10^{\circ}$ C, at $x/L=10^{\circ}$ C and decreases slowly to $T=10^{\circ}$ C, at $x/L=10^{\circ}$ C and decreases slowly to $T=10^{\circ}$ C, at $x/L=10^{\circ}$ C and decreases slowly to $T=10^{\circ}$ C and $T=10^{\circ}$ C C 0.37. It then rises slowly to a local maximum value of $T = 82.3^{\circ}$ C at x/L=0.49. The maximum pressure was $T=85^{\circ}$ C, at x/L=0.94.

Furthermore, the growth rate, b (s⁻¹) of contact pressure by varying the conductivity $K_{22}=1,2,3,4\mathrm{W/(m\cdot K)}$ were found to be 0.4374, 0.4004, 0.374 and 0.2650, respectively. The resulting growth rate explains the contact pressure behavior as evident in Fig. 7. Moreover, as the growth rate decreases, the critical sliding speed of the system increases leading to a more stable system.

5.2. Effect of elastic modulus

The prior research works have shown that materials with high elastic modulus encourage the formations of hotspots and the subsequent result is system instability. Moreover, works on the elasticity of materials

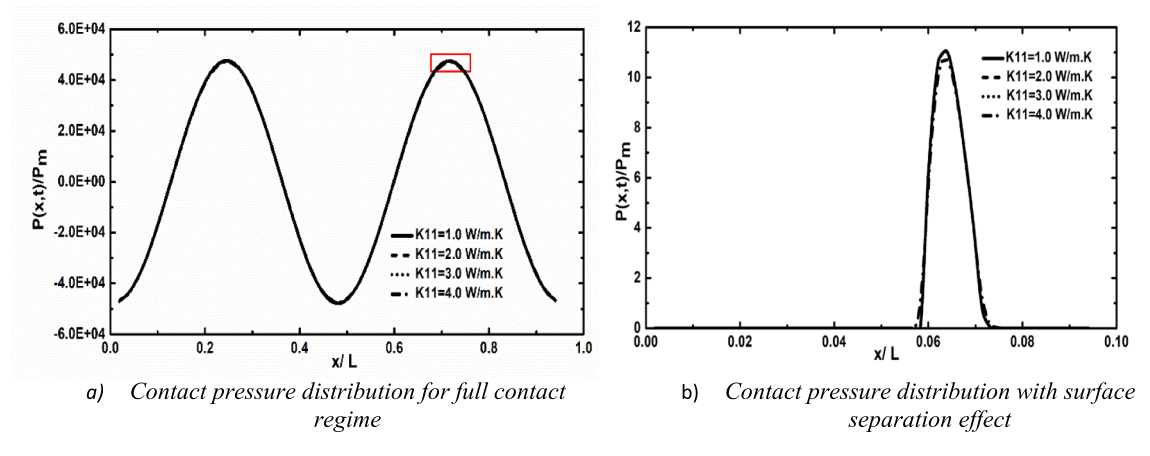


Fig. 6. Surface contact pressure distribution for thermal conductivity in the longitudinal direction: a) full contact regime b) with separation effect.

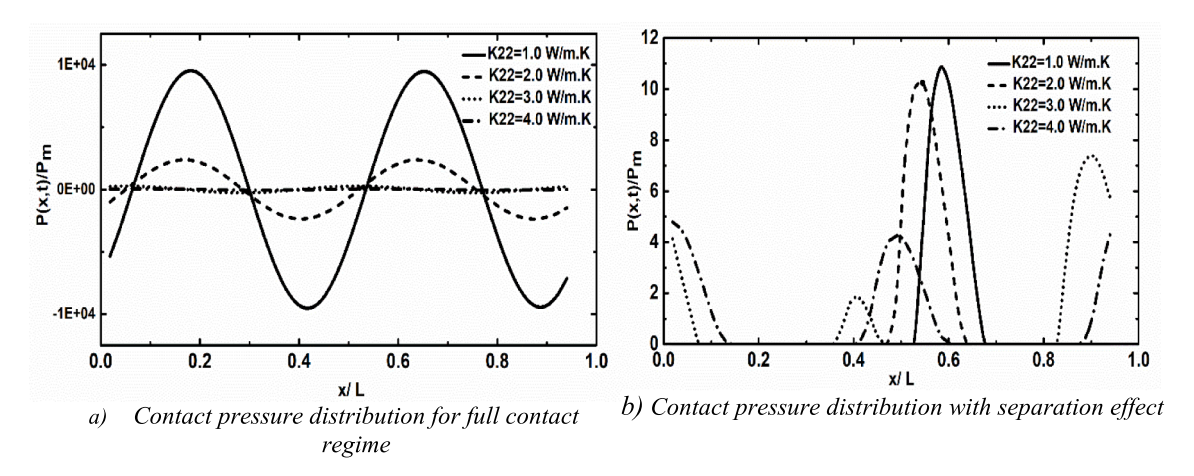


Fig. 7. Surface contact pressure distribution for thermal conductivity in the transverse direction a) full-contact regime b) with separation effect.

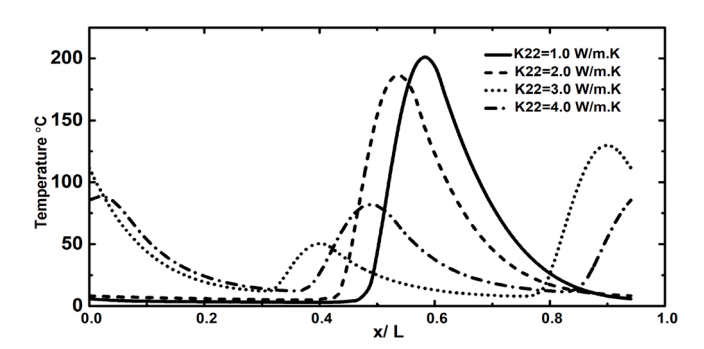


Fig. 8. Temperature distribution along the contact interface for thermal conductivity in the transverse direction with separation effect.

whose properties are not invariant with respect to direction and how they contribute to TMI formation are lacking in research. This study investigated the unstable behavior of the friction material caused by the elastic modulus in the longitudinal E_{11} and thickness direction E_{22} .

5.2.1. Longitudinal direction (E_{11})

From Table 1, K_{11} , K_{22} , E_{22} , α_{11} , α_{22} were held constant at 4 W/(m·K), 4 W/(m·K) 11GPa, 13 μ C⁻¹, 13 μ C⁻¹ respectively while changing the elasticity ($E_{11}=9,10,11,12$ GPa) for the TMI analysis with and without the surface separation effect. The resulting contact pressure distributions are shown in Fig. 9a & b respectively. It is noteworthy that, for the full-contact regime (no separation) as seen in Fig. 9a, the maximum

contact pressure increases as the elastic modulus E_{11} is increased except for $E_{11} = 11$. This occurs because the problem becomes non-linear at a certain period. Further restricting the problem to be linear through out the iterative process leads to no separation at the contact surface, causing continuous heat generation at the contact interface. This makes it difficult to predict the actual behavior of the system at extremely high temperatures since the contact is constrained. For this reason, it is important to consider the non-linear case by introducing contact with the separation effect. Conversely, the maximum pressure was found to decrease as E_{11} increased. This is expected because, at a steady-state, the temperature may cease to grow unlike in the case of a full-contact regime due to the non-linearity of the problem. Moreover, the corresponding growth rate, $b(s^{-1})$ by increasing $E_{11} = 9, 10, 11, 12$ GPa was found to decrease slightly: 0.256, 0.2366, 0.218 and 0.215, respectively. This indicates that there is an increase in the critical velocity by increasing E_{11} . Also, the corresponding temperature distributions show that there is a slight reduction in the maximum temperature from T =211.25°C to T = 206°C as E_{11} is increased. It can also be deduced that the uniformity of temperature is improved slightly by increasing E_{11} .

5.2.2. Transverse direction (E_{22})

Fig. 10a & b show the evolution of contact pressure distribution for full contact regime and with separation effect respectively by varying the elastic modulus in the thickness direction ($E_{22}=9,10,11,12$ GPa) while keeping all other parameters constant as carried out in Section 5.2.1. The results revealed that the elastic modulus in the thickness direction significantly promotes TMI formation. Increasing E_{22} for a full-contact regime caused the contact pressure to grow rapidly. Similar

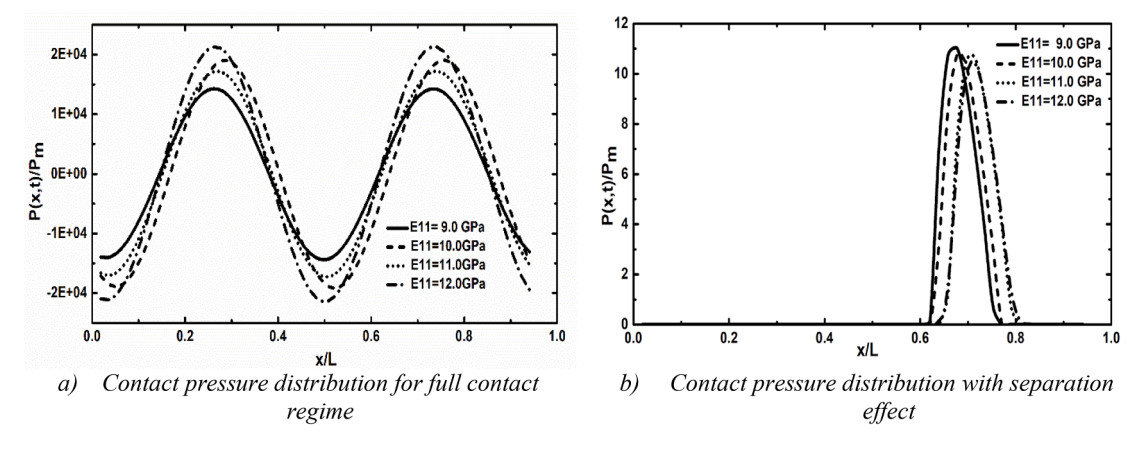


Fig. 9. Surface contact pressure distribution for elastic modulus in the longitudinal direction a) full contact regime b) with separation effect.

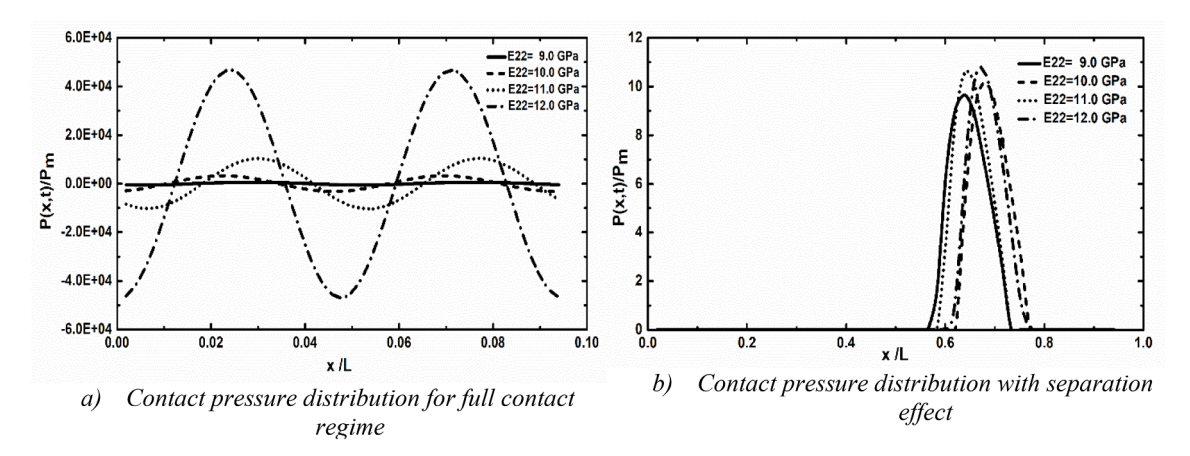


Fig. 10. Contact pressure distribution for elastic modulus in the transverse direction a) full-contact regime b) with separation effect.

behavior is observed for contact with the separation effect except that the growth was gradual as seen in Fig. 10b. The corresponding growth rates b (s $^{-1}$) by increasing $E_{22}=9,10,11,12$ GPa were found to be 0.094, 0.111, 0.190 and 0.215, respectively. The resulting growth rates show that the critical sliding speed decreases as E_{22} is increased. This can be attributed to the fact that the thickness direction of the material dominates, leading to higher contact pressure and thus a higher frictional heat generation, thus making the friction material more susceptible to TMI.

5.3. Effect of coefficient of thermal expansion

5.3.1. Longitudinal direction (α_{11})

Similarly, the thermal expansion in the longitudinal direction was varied ($\alpha_{11}=10,11,12,13\,\mu\text{C}^{-1}$) while keeping $K_{11},K_{22},E_{11},E_{22},\alpha_{22}$ constant at 4 W/(m·K), 4 W/(m·K),11GPa,11GPa, 13.10^{-6}C^{-1} respectively. In this analysis, only contact with the separation effect was considered. It was observed that instability is promoted slightly by increasing the coefficient of thermal expansion α_{11} as seen in Fig. 11. The corresponding growth rates (s^{-1}) were 0.0374, 0.0375,0.0378, and 0.0380, respectively. Overall, the influence of thermal expansion in the sliding direction was not significant.

5.3.2. Transverse direction (α_{22})

The same process was repeated for the coefficient of thermal expansion $(\alpha_{22}=10,11,12,13\,\mu\text{C}^{-1})$ in the thickness direction. The maximum peak values of the perturbation $(P(x,t)/P_m)$ for each varied coefficient of thermal expansion were almost constant as seen in Fig. 12. The corresponding growth rates by increasing $\alpha_{22}=10,11,12,13\,\mu\text{C}^{-1}$

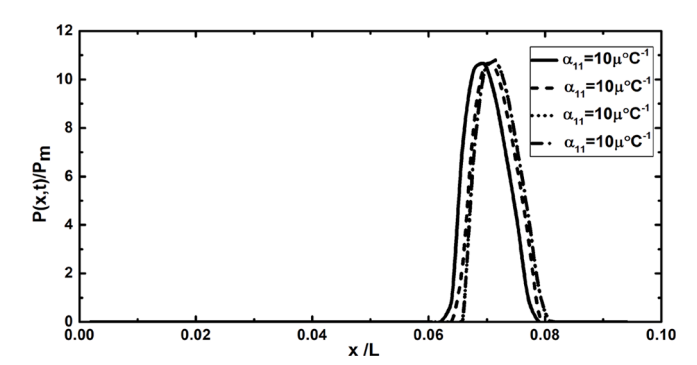


Fig. 11. Surface contact pressure distribution for the coefficient of thermal expansion in the longitudinal direction.

were found to be 0.03733, 0.03734, 0.0374 and 0.03745, respectively. In other words, the coefficient of thermal expansion of the friction material in the thickness direction has a negligible effect on the formation of TMI.

6. Conclusions

A thermomechanical model was developed to investigate the effects of the elastic modulus, thermal conductivity, and coefficient of thermal expansion in the sliding and thickness directions of a metal-free friction material on TMI. The model was validated using an existing eigenvalue approach. The results for a full-contact regime and contact with the surface separation effect are investigated and the results are discussed.

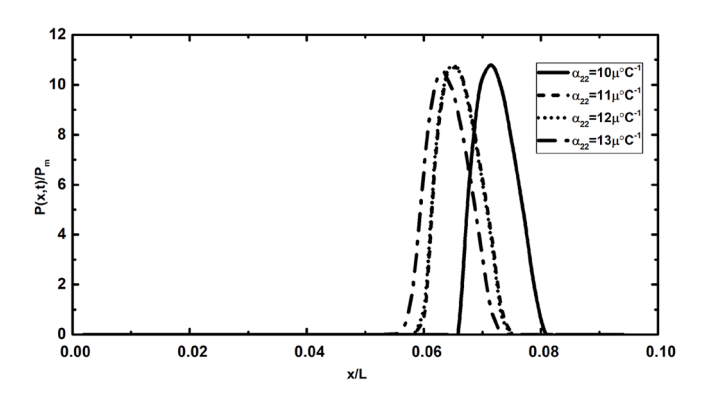


Fig. 12. Surface contact pressure distribution for the coefficient of thermal expansion in the transverse direction.

Increasing the elastic modulus E_{11} and thermal conductivity K_{22} were found to discourage TMI formation during interactions. Conversely, increasing the thermal conductivity K_{11} and Elastic modulus E_{22} were found to make the friction material more susceptible to TMI formation. Furthermore, the coefficient of thermal expansion in the sliding direction was found to promote TMI formation slightly. Meanwhile, in the thickness direction, it appears to have a negligible effect on the thermomechanical deformation. In general, manufacturers of automotive disc clutch and brake pads must optimize the material properties of metal-free friction materials to address the issue of thermomechanical instability in automotive disc brake pads and clutches.

Data availability

All data generated or analyzed during this study are included in this published article.

Funding

Support for this work, provided by the National Science Foundation under Contract (No. 1928876), is gratefully acknowledged.

Declaration of Competing Interest

The authors declare the following financial interests/personal relationships which may be considered as potential competing interests: Yi Yun-Bo reports financial support was provided by National Science Foundation.

References

Al-Shabibi, A.M., Barber, J.R., 2002. Transient solution of a thermoelastic instability problem using a reduced-order model. Int. J. Mech. Sci. 44, 451–464. https://doi. org/10.1016/S0020-7403(01)00110-2.

- Anderson, A.E., Knapp, R.A., 1990. Hot spotting in automotive friction systems. Wear 135, 319–337. https://doi.org/10.1016/0043-1648(90)90034-8.
- Azarkhin, A., Barber, J.R., 1986. Thermoplastic Instability for the Transient Contact Problem of Two Sliding Half-Planes. J. Appl. Mech. 53, 565–572. https://doi.org/ 10.1115/1.3171812
- Barber, J.R., 1969. Thermoelastic instabilities in the sliding of conforming solids. Proc. R. Soc. Lond. A 312, 381–394. https://doi.org/10.1098/rspa.1969.0165.
- Biczó, R., Kalácska, G., Mankovits, T., 2020. Micromechanical Model and Thermal Properties of Dry-Friction Hybrid Polymer Composite Clutch Facings. Materials 13, 4508. https://doi.org/10.3390/ma13204508.
- Burton, R.A., Nerlikar, V., Kilaparti, S.R., 1973. Thermoplastic instability in a seal-like configuration 12.
- Chiou, H., 2019. Copper Toxicity and Prediction Models of Copper Content in Leafy Vegetables. Sustainability 11, 6215. https://doi.org/10.3390/su11226215.
- Dow, T.A., Burton, R.A., 1972. Thermoelastic instability of sliding contact in the absence of wear. Wear 19, 315–328. https://doi.org/10.1016/0043-1648(72)90123-8.
- Heinrich, J.C., Huyakorn, P.S., Zienkiewicz, O.C., Mitchell, A.R., 1977. An 'upwind' finite element scheme for two-dimensional convective transport equation. Int. J. Numer. Meth. Eng. 11, 131–143. https://doi.org/10.1002/nme.1620110113.
- Jang, J.Y., Khonsari, M.M., 2003. A Generalized Thermoelastic Instability Analysis. Proceedings: Mathematical. Phys. Eng. Sci. 459 (2030), 309–329.
- Jang, J.Y., Khonsari, M.M., 1999. Thermoelastic Instability Including Surface Roughness Effects. J. Tribol. 121, 648–654. https://doi.org/10.1115/1.2834118.
- Kao, T.K., Richmond, J.W., Douarre, A., 2000. Brake disc hot spotting and thermal judder: an experimental and finite element study. Int. J. Veh. Des. 23, 276–296
- Kennedy Jr., F.E., Ling, F.F., 1974. Closure to "Discussions of 'A Thermal, Thermoelastic, and Wear Simulation of a High-Energy Sliding Contact Problem" (1974, ASME J. Lubr. Technol., 96, pp. 505–506). J. Lubr. Technol. 96, 507. https://doi.org/10.1115/1.3452029.
- Koranteng, K., Shaahu, J.-S., Chengnan, M.a., Li, H., Yi, Y.-B., 2021a. The performance of Cu-based friction material in dry clutch engagement. Proc. Inst. Mech. Eng. Part J: J. Eng. Tribol. 235 (6), 1114–1123.
- Koranteng, K., Shaahu, J.-S., Yi, Y.-B., 2021b. Effect of contact geometry on temperature field distribution and thermal buckling of an in-wheel disc brake system. Aust. J. Mech. Eng. 1–13 https://doi.org/10.1080/14484846.2021.1958992.
- Lee, K., Barber, J.R., 1993. Frictionally Excited Thermoelastic Instability in Automotive Disk Brakes. J. Tribol. 115, 607-614. https://doi.org/10.1115/1.2921683.
- Lee, K., Dinwiddie, R.B., 1998. Conditions of Frictional Contact in Disk Brakes and their Effects on Brake Judder, in: SAE Technical Paper. SAE International. https://doi.org/ 10.4271/980598.
- Li, J., Barber, J.R., 2008. Solution of transient thermoelastic contact problems by the fast speed expansion method. Wear 265, 402–410. https://doi.org/10.1016/j. wear.2007.11.010.
- Malhotra, N., Ger, T.-R., Uapipatanakul, B., Huang, J.-C., Chen, K.-H.-C., Hsiao, C.-D., 2020. Review of Copper and Copper Nanoparticle Toxicity in Fish. Nanomaterials 10, 1126. https://doi.org/10.3390/nano10061126.
- Smith, M., 2009. ABAQUS/Standard User's Manual, Version 6.9. Dassault Systèmes Simulia Corp, United States.
- Yi, Y.B., Barber, J.R., Zagrodzki, P., 2000. Eigenvalue solution of thermoelastic instability problems using Fourier reduction. Proc. R. Soc. Lond. A 456, 2799–2821. https://doi.org/10.1098/rspa.2000.0641.
- Yi, Y.B., Barber, J.R., 2001. HotSpotter: A windows-based software package for solving thermoelastic instabilities in high-speed sliding systems. The Regents of the University of Michigan, License No.1867.
- Yu, C.-C., Heinrich, J.C., 1987. Petrov—Galerkin method for multidimensional, time-dependent, convective-diffusion equations. Int. J. Numer. Meth. Eng. 24, 2201–2215. https://doi.org/10.1002/nme.1620241112.
- Zagrodzki, P., 1990. Analysis of thermomechanical phenomena in multidisc clutches and brakes. Wear 140, 291–308. https://doi.org/10.1016/0043-1648(90)90091-N.
- Zagrodzki, P., Lam, K.B., Al Bahkali, E., Barber, J.R., 2001. Nonlinear Transient Behavior of a Sliding System With Frictionally Excited Thermoelastic Instability. J. Tribol. 123, 699–708. https://doi.org/10.1115/1.1353180.
- Zhao, J., Yi, Y.B., Li, H., 2015. Effects of frictional material properties on thermoelastic instability deformation modes. Proc. Inst. Mech. Eng. Part J: J. Eng. Tribol. 229, 1239–1246. https://doi.org/10.1177/1350650115576783.